REPORT DOCUMENTATION PAGE

Form Approved
OMB NO. 0704-0188

1. AGENCY USE ONLY (Leave Blank)	2. REPORT DATE	3. REPORT TYPE AND DATES COVERED
	31 May 2007	01 August, 06 – 30 April 07

4. TITLE AND SUBTITLE

Hearing Protection for High-Noise Environments

5. FUNDING NUMBERS
FA9550-06-C-0034

6. AUTHOR(S)
Elizabeth Bleszynski, Marek Bleszynski, Thomas Jaroszewicz

7. PERFORMING ORGANIZATION NAME(S) AND ADDRESS(ES)
Monopole Research
739 Calle Sequoia, Thousand Oaks, CA 91360

8. PERFORMING ORGANIZATION REPORT NUMBER
MON0003

9. SPONSORING / MONITORING AGENCY NAME(S) AND ADDRESS(ES)

Air Force Office of Scientific Research
875 North Randolph Rd., Room 3112
Arlington, VA 22203

10. SPONSORING / MONITORING AGENCY REPORT NUMBER

11. SUPPLEMENTARY NOTES

The views, opinions and/or findings contained in this report are those of the author(s) and should not be construed as an official Department of the Air Force position, policy or decision, unless so designated by other documentation.

12 a. DISTRIBUTION / AVAILABILITY STATEMENT

Approved for public release, distribution unlimited.

12 b. DISTRIBUTION CODE

13. ABSTRACT (Maximum 200 words)

Report developed under STTR contract for topic AF06-T035.

The objective of our effort was to develop powerful software tools and to perform high fidelity simulation which would allow identification and understanding of relevant bioacoustic and psychoacoustic mechanisms responsible for the transmission of acoustic energy through non-airborne pathways to the cochlea.

As the main achievements of our Phase I work we consider:

- development of a set of algorithms (including non-lossy, error-controlled matrix compression techniques) for general, i.e., variable-density, volumetric equations of acoustics, and

- development of a solution technique overcoming ill-conditioning difficulties arising in large density contrast problems.

14. SUBJECT TERMS

STTR report, bone conducted sound, computational acoustics, integral equations, FFT–based matrix compression

15. NUMBER OF PAGES
part I : V + 53
part II: III + 43

16. PRICE CODE

17. SECURITY CLASSIFICATION OR REPORT	18. SECURITY CLASSIFICATION ON THIS PAGE	19. SECURITY CLASSIFICATION OF ABSTRACT	20. LIMITATION OF ABSTRACT
UNCLASSIFIED	**UNCLASSIFIED**	**UNCLASSIFIED**	**UL**

NSN 7540-01-280-5500

Standard Form 298 (Rev.2-89)
Prescribed by ANSI Std. 239-18
298-102

20070911046

GENERAL INSTRUCTIONS FOR COMPLETING SF 298

The Report Documentation Page (RDP) is used for announcing and cataloging reports. It is important that this information be consistent with the rest of the report, particularly the cover and title page. Instructions for filling in each block of the form follow. It is important to ***stay within the lines*** to meet ***optical scanning requirements.***

Block 1. Agency Use Only (Leave blank)

Block 2. Report Date. Full publication date including day, month, and year, if available (e.g. 1 Jan 88). Must cite at least year.

Block 3. Type of Report and Dates Covered. State whether report is interim, final, etc. If applicable enter inclusive report dates (e.g. 10 Jun 87 - 30 Jun 88).

Block 4. Title and Subtitle. A title is taken from the part of the report that provides the most meaningful and complete information. When a report is prepared in more than one volume, repeat the primary title, and volume number, and include subtitle for the specific volume. On classified documents enter the title classification in parentheses.

Block 5. Funding Numbers. To include contract and grant numbers; may include program element number(s) project number(s), task number(s), and work unit number(s). Use the following labels:

C - Contract	**PR** - Project
G - Grant	**TA** - Task
PE - Program Element	**WU** - Work Unit Accession No.

Block 6. Author(s). Name(s) of person(s) responsible for writing the report, performing the research, or credited with the content of the report. If editor or compiler, this should follow the name(s).

Block 7. Performing Organization Name(s) and Address(es). Self-explanatory.

Block 8. Performing Organization Report Number. Enter the unique alphanumeric report number(s) assigned by the organization performing the report.

Block 9. Sponsoring/Monitoring Agency Name(s) and Address(es) Self-explanatory.

Block 10. Sponsoring/Monitoring Agency Report Number. *(if known)*

Block 11. Supplementary Notes. Enter information not included elsewhere such as; prepared in cooperation with....; Trans. of...; To be published in.... When a report is revised, include a statement whether the new report supersedes or supplements the older report.

Block 12a. Distribution/Availability Statement. Denotes public availability or limitations. Cite any availability to the public. Enter additional limitations or special markings in all capitals (e.g. NORFORN, REL, ITAR).

DOD	- See DoDD 4230.25, "Distribution Statements on Technical Documents."
DOE	- See authorities.
NASA	- See Handbook NHB 2200.2.
NTIS	- Leave blank.

Block 12b. Distribution Code.

DOD	- Leave Blank
DOE	- Enter DOE distribution categories from the Standard Distribution for unclassified Scientific and Technical Reports
NASA	- Leave Blank.
NTIS	- Leave Blank.

Block 13. Abstract. Include a brief (*Maximum 200 words)* factual summary of the most significant information contained in the report.

Block 14. Subject Terms. Keywords or phrases identifying major subject in the report.

Block 15. Number of Pages. Enter the total number of pages.

Block 16. Price Code. Enter appropriate price code (NTIS *only*).

Block 17. - 19. Security Classifications. Self-explanatory. Enter U.S. Security Regulations (i.e., UNCLASSIFIED). If form contains classified information, stamp classification on the top and bottom of the page.

Block 20. Limitation of Abstract. This block must be completed to assign a limitation to the abstract. Enter either UL (Unlimited) or SAR (same as report). An entry in this block is necessary if the abstract is to be limited. If blank, the abstract is assumed to be unlimited.

MASTER COPY: PLEASE KEEP THIS "MEMORANDUM OF TRANSMITTAL" BLANK FOR REPRODUCTION PURPOSES. WHEN REPORTS ARE GENERATED UNDER THE ARO SPONSORSHIP, FORWARD A COMPLETED COPY OF THIS FORM WITH EACH REPORT SHIPMENT TO THE ARO. THIS WILL ASSURE PROPER IDENTIFICATION. NOT TO BE USED FOR INTERIM PROGRESS REPORTS; SEE PAGE 2 FOR INTERIM PROGRESS REPORT INSTRUCTIONS.

MEMORANDUM OF TRANSMITTAL

U.S. Army Research Office
ATTN: AMSRL-RO-BI (TR)
P.O. Box 12211
Research Triangle Park, NC 27709-2211

☐ Reprint (Orig + 2 copies)

☐ Technical Report (Orig + 2 copies)

☐ Manuscript (1 copy)

☐ Final Progress Report (Orig + 2 copies)

☐ Related Materials, Abstracts, Theses (1 copy)

CONTRACT/GRANT NUMBER:

REPORT TITLE:

is forwarded for your information.

SUBMITTED FOR PUBLICATION TO (applicable only if report is manuscript):

Sincerely,

Phase I Final Report, Part II

HEARING PROTECTION FOR HIGH-NOISE ENVIRONMENTS
Finite Element Modeling

Contract # **FA9550-06-C-0034**

Topic # **AF06-T035**

Period of Performance: **August 01, 2006 - April 30, 2007**

Prepared by:

Institute for Computational Engineering and Sciences
University of Texas at Austin

Contents

List of Figures

List of Tables

1 Introduction

Hearing impairment remains the primary disability among military personnel. Sound pressure levels caused by proximity to aircraft engines or impulse noise from large caliber weapons may easily exceed the pain threshold value of 100 dB.

The focus of this project is to to develop a reliable numerical model for investigating the bone-conducted sound in the human head. The problem is difficult because of a lack of fundamental knowledge regarding the transmission of acoustic energy through non-airborne pathways to the cochlea. A fully coupled model based on the acoustic/elastic interaction problem with a detailed resolution of the cochlea region and its interface with the skull and the air pathways, should provide an insight into this fundamental, long standing research problem.

The project builds on an interaction of experts in numerical wave propagation – Drs. Elizabeth and Marek Bleszynski from Monopole Research with a team at the University of Texas headed by Dr. Leszek Demkowicz and including two experts on wave propagation and hearing science: Dr. Mark Hamilton and Dr. Greg Champlin.

2 The Head Problem

In this section we review shortly specifics of the head problem. The problem falls into the category of general coupled elasticity/acoustics problems discussed in Appendix A with a few minor modifications. The domain Ω in which the problem is defined is the interior of a ball including a model of the human head, and it is split into an acoustic part Ω_a, and an elastic part Ω_e. Depending upon a particular example we shall study, the acoustic part Ω_a includes:

- air surrounding the human head, bounded by the head surface and a truncating sphere; this part of the domain may include portions of air ducts leading to the middle ear through mouth and nose openings;
- cochlea,
- an additional layer of air bounded by the truncating sphere and the outer sphere terminating the computational domain, where the equations of acoustics are replaced with the corresponding *Perfectly Matched Layer* (PML) modification.

The elastic part of the domain includes:

- skull,
- tissue.

By the term *tissue* we understand here all parts of the head that are not occupied by the skull (bone) and the cochlea. This includes the thin layer of the skin and the entire interior of the head with the brain. We will assume that the elastic constants for the whole tissue domain are the same. As the viscosity constant for the tissue is four orders of magnitude smaller than that for the skull, an alternative approach would be to model the tissue as an acoustical fluid, neglecting the shear waves in the brain.

The acoustic wave is represented as the sum of an incident wave p^{inc} and a scattered wave p. Only the scattered wave is assumed to satisfy the radiation (Sommerfeld) condition,

$$\frac{\partial p}{\partial r} + ikp \in L^2(\mathbb{R}^3) \tag{2.1}$$

The different types of boundaries discussed in Appendix A reduce only to the interface between the elastic and acoustic subdomains, and the outer Dirichlet boundary for the acoustic domain. Material interfaces between the skull and tissue, as well between the air and the PML air do not require any special treatment.

The final formulation of the problem has the form A.11, with the bilinear and linear forms defined as follows.

$$\begin{aligned}
b_{ee}(\boldsymbol{u},\boldsymbol{v}) &= \int_{\Omega_e} \left(E_{ijkl}u_{k,l}v_{i,j} - \rho_s\omega^2 u_i v_i\right)\, d\boldsymbol{x} \\
b_{ae}(p,\boldsymbol{v}) &= \int_{\Gamma_I} pv_n\, dS \\
b_{ea}(\boldsymbol{u},q) &= -\omega^2\rho_f \int_{\Gamma_I} u_n q\, dS \\
b_{aa}(p,q) &= \int_{\Omega_a} \left(\boldsymbol{\nabla} p \boldsymbol{\nabla} q - k^2 pq\right)\, d\boldsymbol{x} \\
l_e(\boldsymbol{v}) &= -\int_{\Gamma_I} p^{inc} v_n\, dS \\
l_a(q) &= 0
\end{aligned} \tag{2.2}$$

material	E[MPa]	ν	ρ[kg/m^3]	c_p[m/s]	c_s[m/s]
tissue (brain)	0.67	0.48	1040	75	15
skull (bone)	6500	0.22	1412	2293	1374
cochlea (water)			1000	1500	
air			1.2	344	

Table 1: Material constants and speed of sound for compressional and shear waves.

A symmetric formulation is enabled by dividing the equations of acoustics with factor $\rho_f \omega^2$,

$$\begin{aligned} b_{ee}(\boldsymbol{u},\boldsymbol{v}) &= \int_{\Omega_e} \left(E_{ijkl} u_{k,l} v_{i,j} - \rho_s \omega^2 u_i v_i\right)\, d\boldsymbol{x} \\ b_{ae}(p,\boldsymbol{v}) &= \int_{\Gamma_I} p v_n \, dS \\ b_{ea}(\boldsymbol{u},q) &= -\int_{\Gamma_I} u_n q \, dS \\ b_{aa}(p,q) &= \tfrac{1}{\omega^2 \rho_f} \int_{\Omega_a} \left(\boldsymbol{\nabla} p \boldsymbol{\nabla} q - k^2 p q\right)\, d\boldsymbol{x} \\ l_e(\boldsymbol{v}) &= -\int_{\Gamma_I} p^{inc} v_n \, dS \\ l_a(q) &= 0 \end{aligned} \tag{2.3}$$

Notice that we refer to the outer normal unit vector $\boldsymbol{n}$ always *locally*, i.e. in the formula for the coupling bilinear form b_{ae} involving elasticity test functions $\boldsymbol{v}$, versor $\boldsymbol{n}$ points outside of the elastic domain, whereas in the formula for the coupling bilinear form b_{ea} involving acoustic test functions q, versor $\boldsymbol{n}$ points outside of the acoustic domain. The normal components v_n and u_n present in the coupling terms are thus opposite to each other, and the formulation is indeed symmetric.

2.1 Material and temporar scales

The material data are summarized in Table 1. For elastic materials, the speed of compressional waves and shear waves is given by the formulas:

$$c_p^2 = \frac{E(1-\nu)}{(1+\nu)(1-2\nu)\rho}, \quad c_s^2 = \frac{E}{2(1+\nu)\rho} \tag{2.4}$$

It is illuminating to begin with an estimate of the magnitude of all terms entering the equations. There are three scales to the problem.

Element scale: h representing a typical element length. Assume $h = 1$[cm] $= 10^{-2}$[m].

Elastic displacement in skull scale: b representing the expected magnitude of the acoustical displacements within the skull. Assuming the air pressure at the level of 100[Pa = N/m^2] (threshold of pain), a simple model of a pressure loaded elastic shell of thickness 1-2[cm] responds with a displacement of order $b = 0.1$[mm]$= 10^{-4}$[m].

Pressure scale: p_0 to be assumed.

The following table represents the order of magnitude of all terms entering the formulation for the coupled problem involving the skull and the air only, for an average frequency of $f = 200$[Hz].

$$\begin{aligned}
\text{elastic stiffness term} &= \mu b^2 h \approx 1 \\
\text{elastic mass term} &= \rho_s \omega^2 b^2 h^3 \approx 10^{-5} \\
\text{coupling term} &= p_0 b h^2 \approx 10^{-8} p_0 \\
\text{acoustic stiffness term} &= \frac{1}{\omega^2 \rho_f} p_0^2 h \approx 10^{-11} p_0 \\
\text{acoustic mass term} &= \frac{1}{c^2 \rho_f} p_0^2 h^3 \approx 10^{-14} p_0^2
\end{aligned} \tag{2.5}$$

Assuming the pressure factor in the range of $p_0 \approx 10^8$, we observe that all but one terms in the formulation vary by two-three orders of magnitudes only. Notice that the assumed scales for displacement and pressure have actually nothing to do with the expected displacement and pressure levels. Assuming that displacements are of order 1 would yield the same result. For convenience, we have also assumed the same order of magnitude for test functions. Again, due to the linearity of the equations, the choice does not matter. The five orders of magnitude difference for the elastic mass term (the subwavelength regime) should not present a problem in double precision computations.

In conclusion, the advantage of the coupled formulation "mixing" primary variables (elastic displacement) with dual variables (pressure), is the possibility of adjusting the scaling to yield terms of the same order. The scaling arguments have been confirmed by monitoring *pivots* reported by

frontal solver when solving examples discussed in the next section. Indeed, the pivots varied by the three-four orders of magnitude only.

2.2 PML modification

In the PML part of the acoustical domain, the bilinear form b_{aa} is modified as follows:

$$b_{aa}(p,q) = \int_{\Omega_{a,PML}} \left(\frac{z^2}{z' r^2} \frac{\partial p}{\partial r} \frac{\partial q}{\partial r} + \frac{z'}{r^2} \frac{\partial p}{\partial \psi} \frac{\partial q}{\partial \psi} + \frac{z'}{r^2 \sin^2 \psi} \frac{\partial p}{\partial \theta} \frac{\partial q}{\partial \theta} \right) r^2 \sin \psi dr d\psi d\theta \tag{2.6}$$

Here r, ψ, θ denote the standard spherical coordinates and $z = z(r)$ is the PML stretching factor defined as follows,

$$z(r) = (1 - \frac{i}{k} \left[\frac{r-a}{b-a} \right]^{\alpha}) r \tag{2.7}$$

Here a is the radius of the truncating sphere, b is the external radius of the computational domain ($b - a$ is thus the thickness of the PML layer), i denotes the imaginary unit, k is the acoustical wave number, and r is the radial coordinate. In computations, all derivatives with respect to spherical coordinates are expressed in terms of the standard derivatives with respect to Cartesian coordinates. In all reported computations, parameter $\alpha = 5$. For a detailed discussion on derivation of PML modifications and effects of higher order discretizations see [9].

3 Numerical Examples

We refer to Appendix B for details on our finite element technology and to Appendix C for a description of the parallel linear solver used in Phase I of this project.

3.1 Verification

The code has been verified by implementing so-called *manufactured solutions*. This is a standard technique in finite elements. We assume an analytical solution of *any form* (the manufactured solution), and use the differential equations for both acoustics and elasticity parts, boundary and interface conditions, to compute the corresponding volume forces and boundary fluxes. The verification is invaluable. By assuming a solution that can be

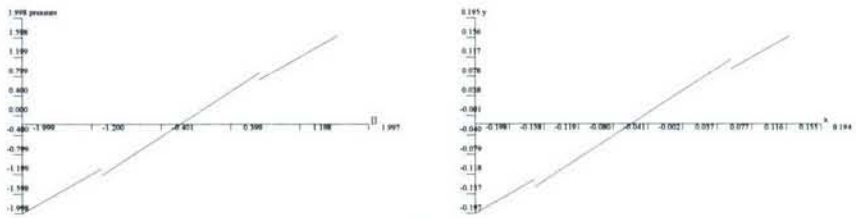

(a) (b)

Figure 1: Verification of the code using a manufactured solution. Pressure distribution along a section passing through the origin and parallel to the x-axis for (a) unit sphere test, and (b) Example 1 with unit material data. Numerical and exact(manufactured) solutions are indistinguishable.

reproduced exactly with the FE shape functions, we do know that the corresponding error must be equal to machine zero, in our case values around 10^{-14}. Any values bigger than these, indicate a bug in the code. Values around 10^{-7} indicate a loss of double precision. In our case, due to the use of linear elements in the acoustic domain and linear or quadratic elements in the elastic part, we can assume any linear variation for pressure, and any linear(quadratic) variation for displacement vector. To verify the code, we have used a simple example of domain consisting of a unit sphere, surrounded with a unit layer of air, and a PML layer of thickness equal to two units. The sphere was meshed with just eight octant tetrahedra, and the air layer with 8×3 tetrahedra obtained by splitting eight prisms, each into three tetrahedra. The PML layer was modeled with two layers of prismatic elements with arbitrary order $p \leq 4$ in the radial direction. All material data were set to O(1) values. A typical result of the verification for a mesh with quadratic elements in the elastic domain, is shown in Fig. 1. The same verification technique was then use to verify each data set and/or the three different solvers used for the project: frontal solver, MUMPS, and the parallel nested dissections multifrontal solver. For small data sets, an additional verification is done by comparing results obtained with the different solvers.

3.2 Phase I Examples

Two numerical examples have been considered in the first phase of the project.

3.2.1 Scattering of a plane wave on an elastic, multilayer sphere

In this model, the domain consists of four concentric spheres. The most inner sphere is filled with an elastic material with data corresponding to human brain. The first layer is also elastic with constants corresponding to human skull. The second layer corresponds to air, and the last one to the PML air. The incident wave is assumed in the form of a plane wave impinging from the top,

$$p^{inc} = p_0 e^{-ik\boldsymbol{e}\cdot\boldsymbol{x}}, \qquad \boldsymbol{e} = (0,0,-1), \qquad p_0 = 1[Pa] \tag{3.1}$$

The test problem is being solved with frequency $f = 200$ Hz. The precise geometry data are as follows:

brain	r <0.1 m
skull	0.1 m $< r <$.125 m
air	0.125 m $< r <$ 0.2 m
PML air	0.2 m $< r <$ 0.3 m

Three tetrahedral meshes for the interior tissue ball, of radius $10cm$,were generated using the simple MATLAB code `distmesh`, described in [6]. The surface of this mesh was then manually extended to generate a skull annulus of thickness $2.5cm$, surrounding air of thickness $7.5cm$, and a PML of thickness $10cm$. The problem was solved on three meshes shown in Figures 2, 3, and 4. . We will refer to them as "small", "big", and "huge" meshes. For all runs discussed for this example, we have used the MUMPS solver.

Fig. 5 displays the distribution of the real part of the pressure over plane $y = 0$ passing through the origin. It looks "good". Unfortunately, a similar picture for the imaginary part reveals a severe instability in the "tissue" region. To double check the VTK graphics, we have displayed the results across a vertical section passing through the origin. The results are shown in Fig. 6. In order to access the problem, we have run the same example but with the Young modulus for the tissue domain increased by two orders of magnitude, i.e. $E = 67$ [MPa]. The corresponding results are shown in Fig. 6. Figure 8 displays the same pressure in dB.

Figures 9 and 10 display the same pressure but this time obtained on the big and huge meshes. The values are at the same level which indicates a converged solution.

Finally, Figures 11 and 12 display the distribution of real and imaginary parts of the pressure over the $y = 0$ section obtained on the big mesh.

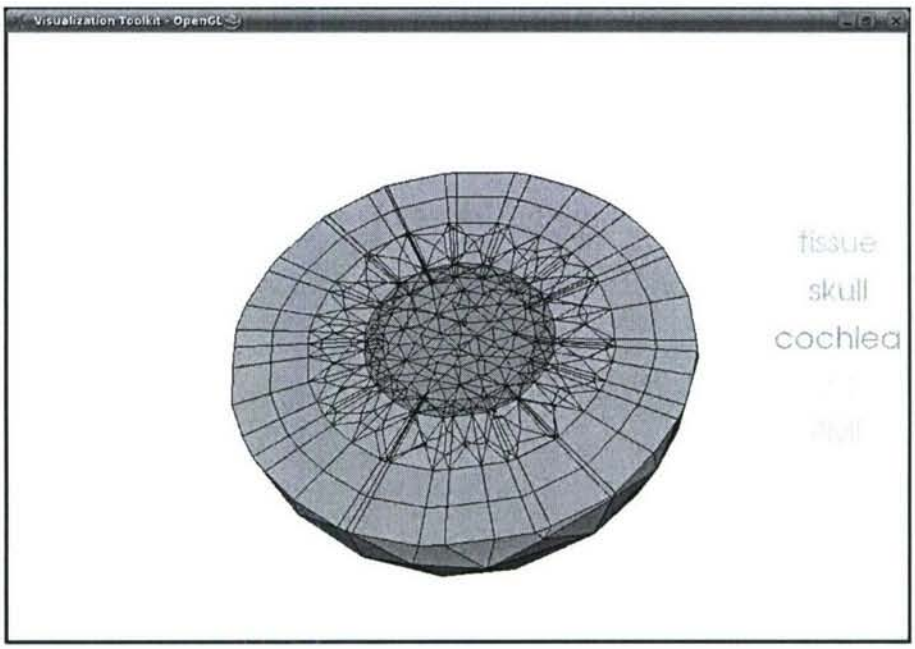

Figure 2: The "small" mesh used to solve the multilayer sphere problem.

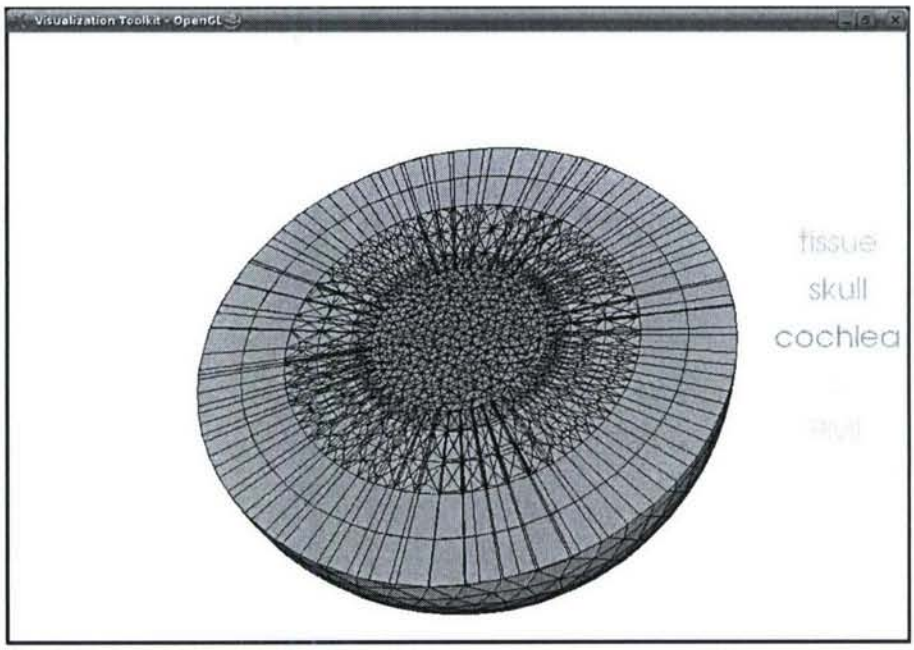

Figure 3: The "big" mesh used to solve the multilayer sphere problem.

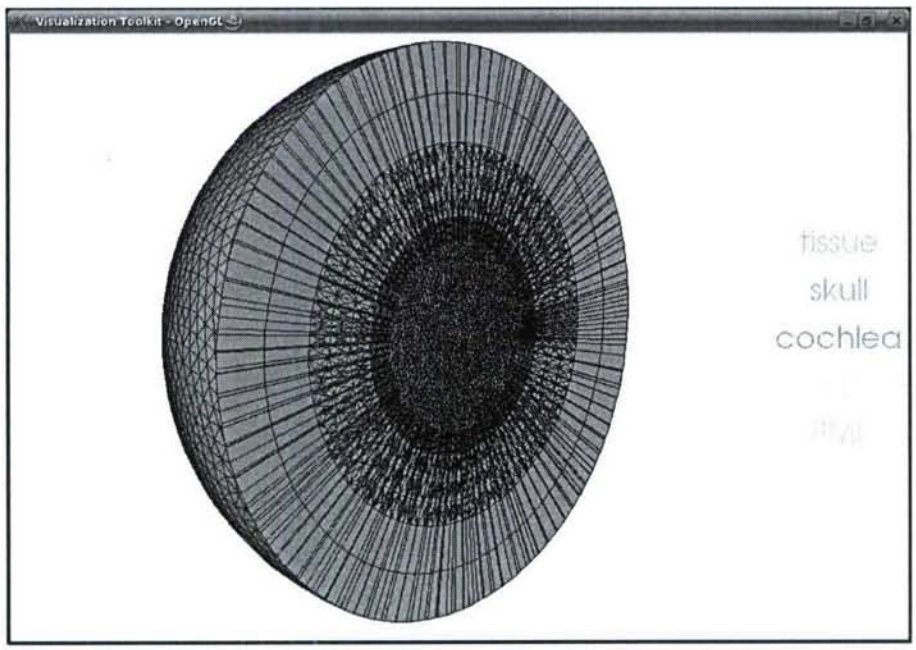

Figure 4: The "huge" mesh used to solve the multilayer sphere problem.

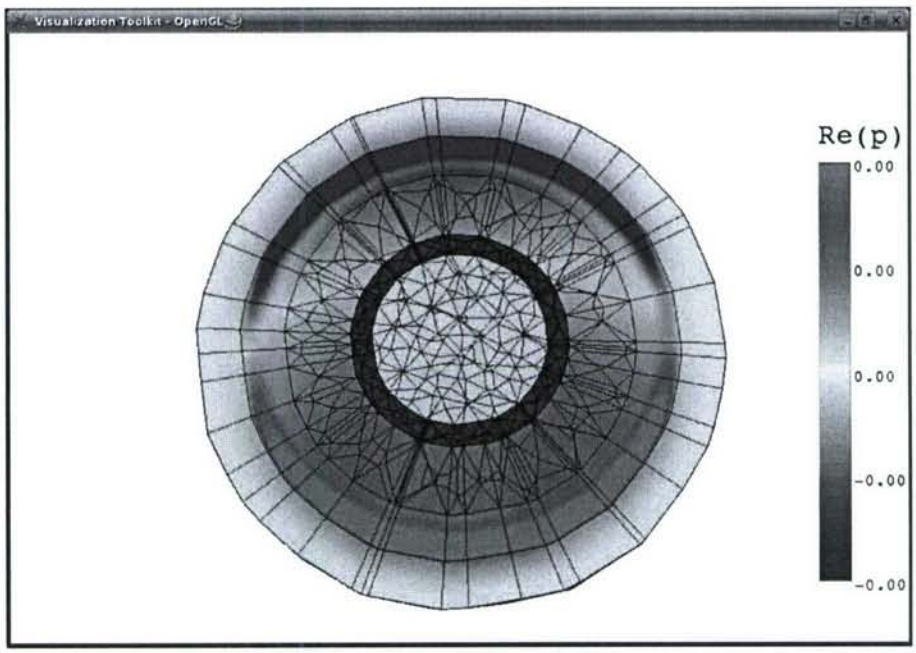

Figure 5: The concentric spheres problem. Small mesh. Plot of real part of pressure on plane $y = 0$ passing through origin.

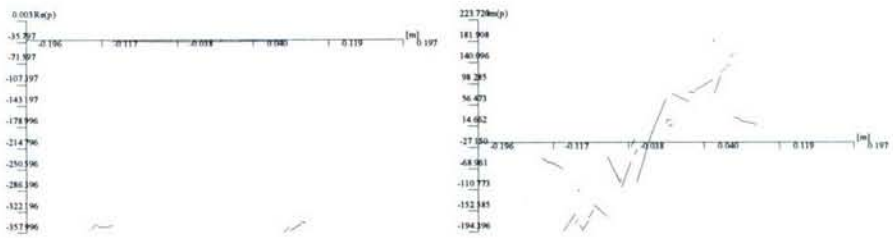

Figure 6: The concentric spheres problem. Small mesh. Plots of real and imaginary part of pressure along the vertical section.

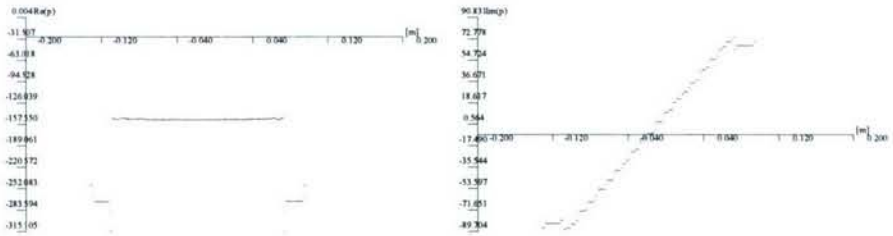

Figure 7: The concentric spheres problem. Small mesh. Plots of real and imaginary part of pressure along the vertical section for the case of a "stiffer" tissue.

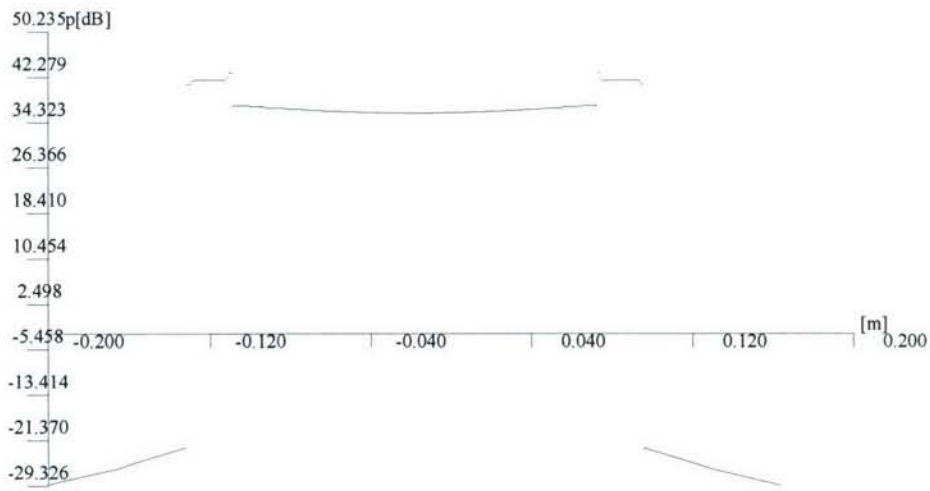

Figure 8: The concentric spheres problem. Small mesh. Plot of pressure along the vertical section in dB for the case of a "stiff" tissue.

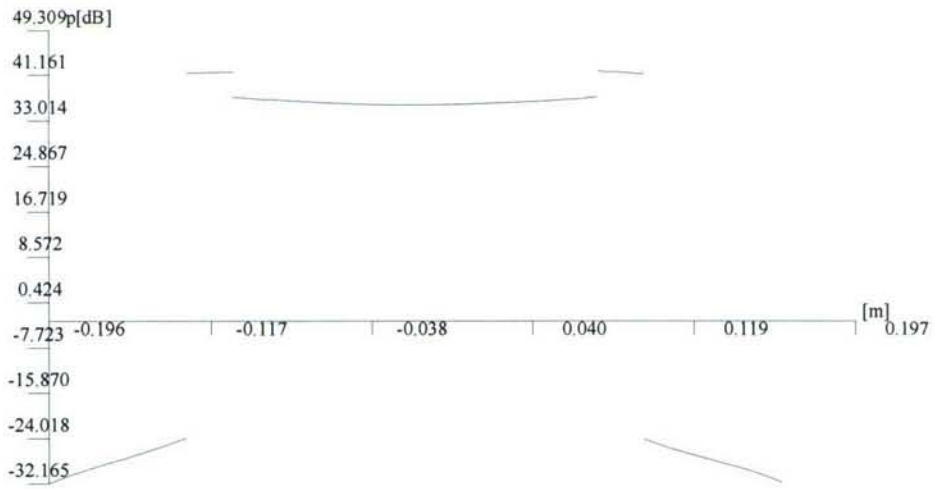

Figure 9: The concentric spheres problem. Big mesh. Plot of pressure along the vertical section in dB for the case of a "stiff" tissue.

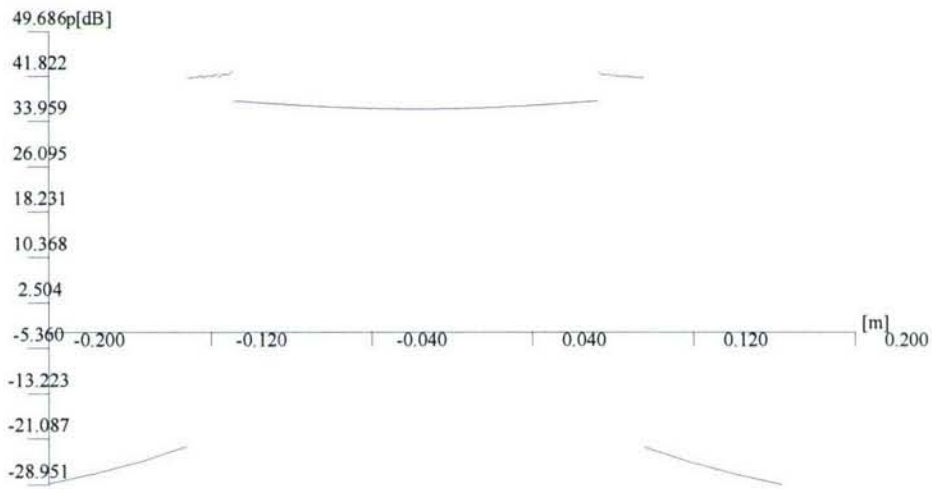

Figure 10: The concentric spheres problem. Huge mesh. Plot of pressure along the vertical section in dB for the case of a "stiff" tissue.

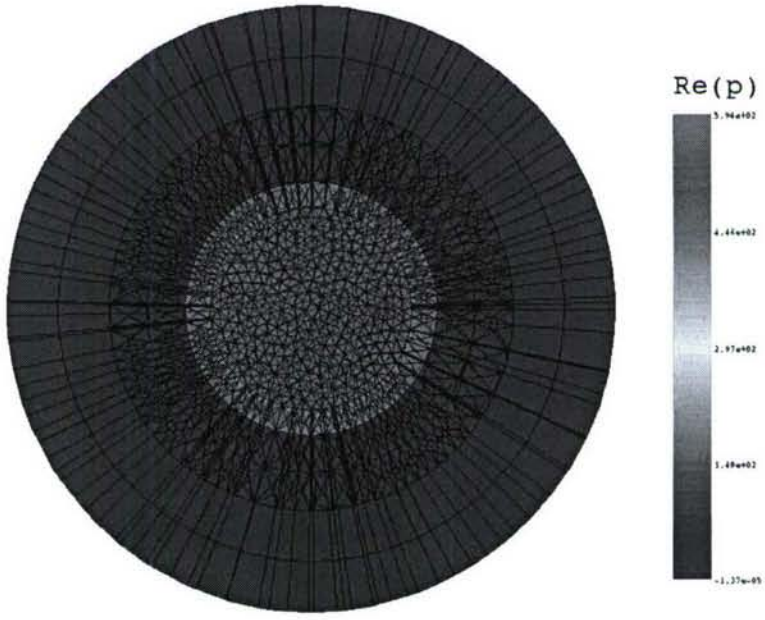

Figure 11: The concentric spheres problem. Big mesh. Plot of real part of pressure on plane $y = 0$ passing through origin.

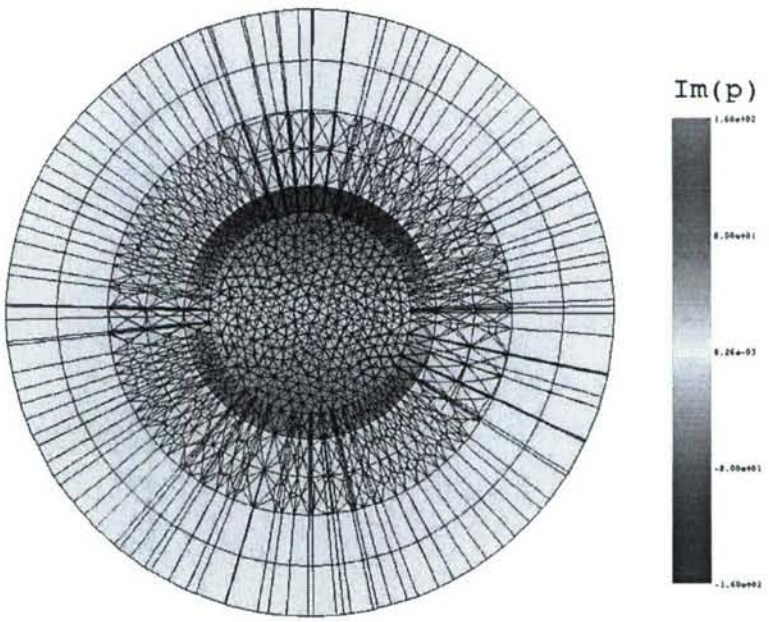

Figure 12: The concentric spheres problem. Big mesh. Plot of imaginary part of pressure on plane $y = 0$ passing through origin.

Figures 13 and 14 display the distribution of real and imaginary parts of the pressure over the $y = 0$ section obtained on the big mesh rescaled to values from -.00001 to .00001 for the real part, and from -.0001 to .0001 for the imaginary part.

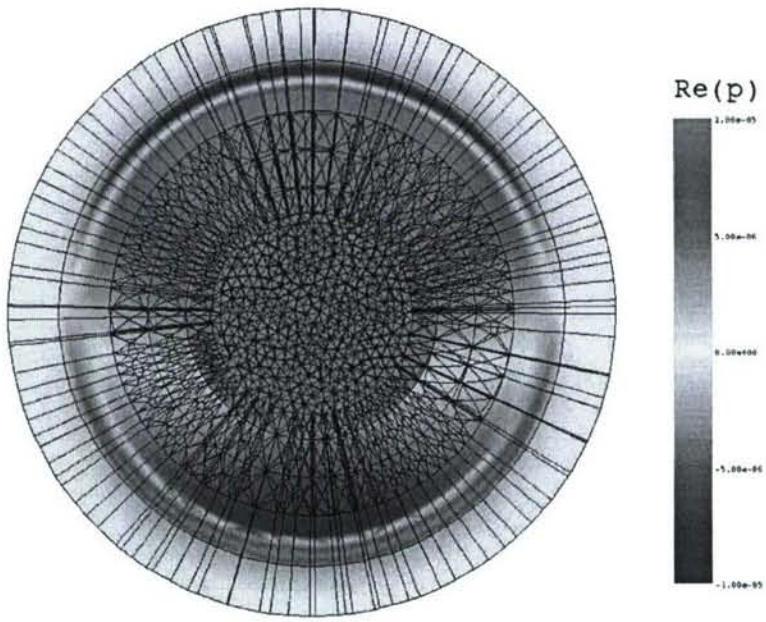

Figure 13: The concentric spheres problem. Big mesh. Plot of real part of pressure on plane $y = 0$ passing through origin, in the range -.00001 to .00001.

The statistics for the largest mesh on which we have succesfully run the code is as follows.

$$\begin{aligned}
\text{number of tets} &= 890144 \\
\text{number of tissue tets} &= 183872 \\
\text{number of skull tets} &= 353136 \\
\text{number of cochlea tets} &= 0 \\
\text{number of air tets} &= 353136 \\
\text{number of PML prisms} &= 16816 \\
\text{total number of d.o.f.} &= 430566
\end{aligned} \tag{3.2}$$

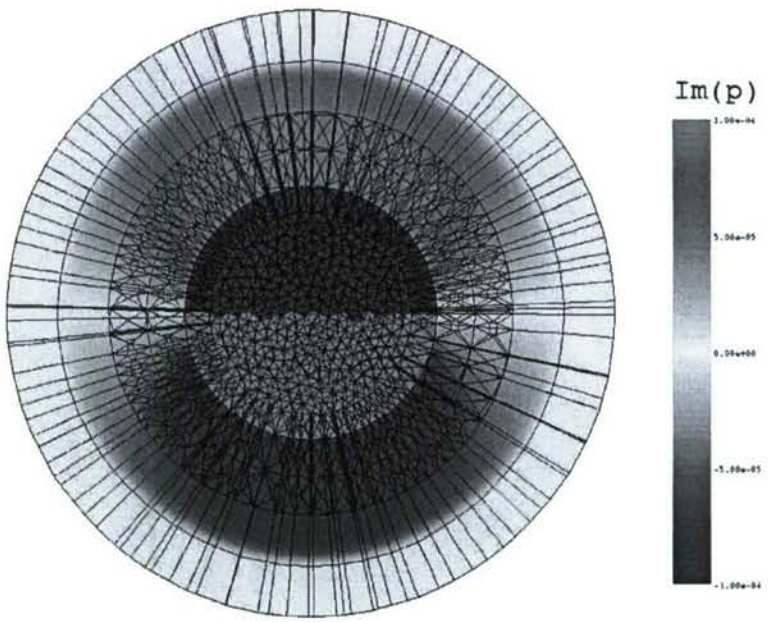

Figure 14: The concentric spheres problem. Big mesh. Plot of imaginary part of pressure on plane $y = 0$ passing through origin, in the range -.0001 to .0001.

3.2.2 Scattering of a plane wave on a "head" with a cochlea

The analysis domains is divided into three subdomains as shown in Figure 15: cochlea, skull, and air. The skull is represented by a spherical shell, and the cochlea is located inside the ear canal represented with a cylindrical cavity. Except cochlea and skull, the remaining part of region within the outer bounding sphere is classified as air. The cochlea is connected with the skull by "growing" manually an additional bone structure in between the skull and the cochlea, i.e. a number of air elements in the cavity is manually reclassified as the skull elements.

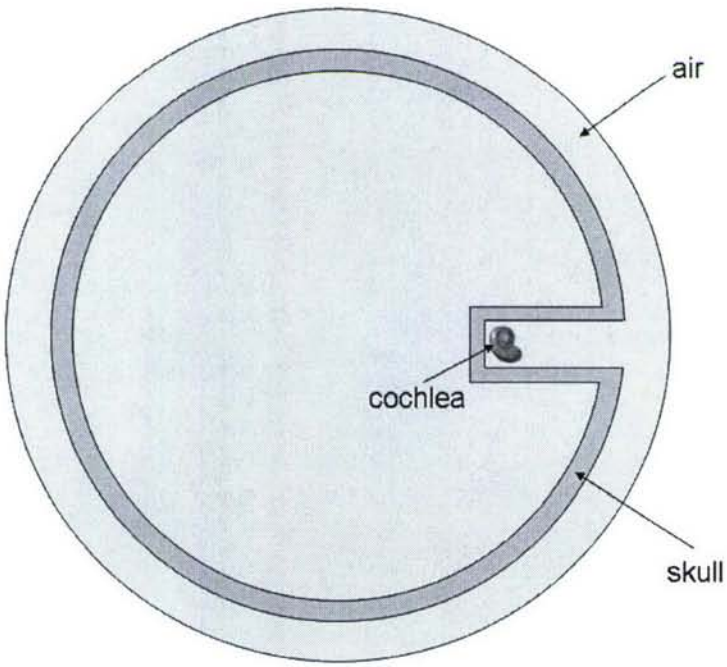

Figure 15: The analysis domain of the human hearing system with three materials: cochlea (yellow), skull (green) and air (blue).

The head is excited with the same plane wave as in the first example. The purpose of this example was to investigate the proportion of the energy transferred to the cochlea directly through air and indirectly through the bone. It took several iterations to generate a FE mesh that captures geometrical details of the cochlea, provides a nessary resolution to resolve the wavelength scales in the "brain", and satifies mesh regularity criteria for the

FE computations (sufficiently large jacobians). The statistics of the mesh is as follows.

$$\begin{aligned} \text{total number of elements} &= 955234 \\ \text{number of tets} &= 878314 \\ \text{number of tissue tets} &= 260800 \\ \text{number of skull tets} &= 304333 \\ \text{number of cochlea tets} &= 13168 \\ \text{number of air tets} &= 300013 \\ \text{total number of d.o.f.} &= 477961 \end{aligned} \tag{3.3}$$

A cross-section through the mesh and details of the meshes of the "ear channel" and the cochlea model are shown in Figures 16, 17 and 18.

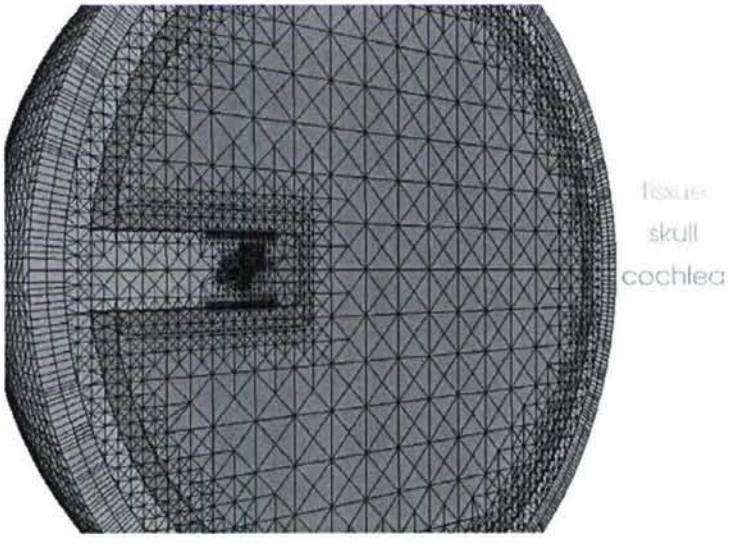

Figure 16: Mesh for the "cochlea problem".

Unfortunately, we have not managed to succesfully run the problem using the MUMPS solver due to memory limitations (the interface with the parallel solver has not been updated yet to quadratic elements).

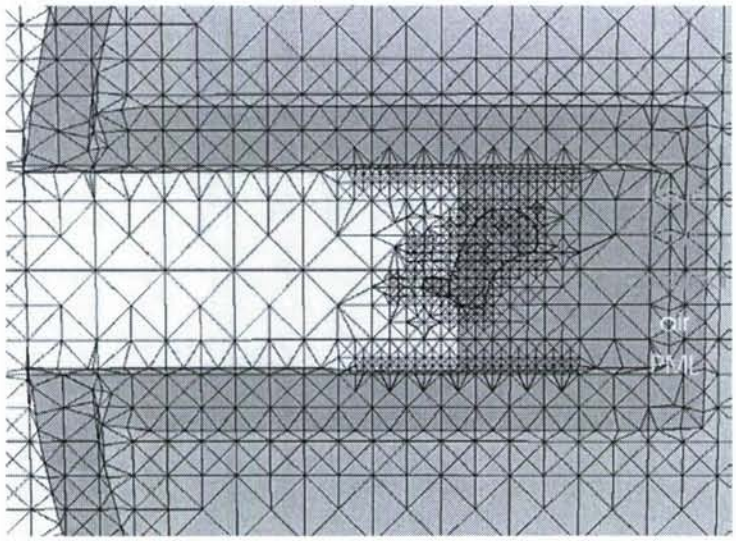

Figure 17: The "cochlea problem". A detail of the mesh in the "ear channel" around the model of cochlea.

Figure 18: The "cochlea problem". Mesh for the cochlea model.

4 Results of Phase I

The following is a short summary of our accomplishments in Phase I of the project.

1. We have developed a mathematical formulation for the coupled problem and the corresponding Galerkin approximation based on hybrid tetrahedral/prismatic meshes.

2. We have developed from scratch a FE code to solve the coupled problem using linear and quadratic tetrahedral elements, and prisms of variable order in the radial direction to handle the PML truncation of the computational domain. The code includes: mesh generator, element routines, an interface with VTK visualization package and interfaces with three linear solvers: an in-house frontal solver, European MUMPS, and a parallel solver. The code consists of over 30,000 lines, excluding the solvers.

3. We have verified the code by using the method of manufactured solutions and comparing results obtained with different solvers.

4. We have succesfully solved the concentric spheres problem for the case of a "stiff tissue" and demonstrated a convergent solution by employing three different meshes with an increasing number of d.o.f.

5. We have generated meshes for the cochlea problem but have not managed to solve it.

6. We have generated meshes for the actual head problem that have been used by the partners at Monopole.

5 Lessons learned from Phase I

Our initial plans were to use our existing three-dimensional *hp*-code based on hexahedral meshes. The code has been in use for many years, and it comes with the possibility of running various adaptive schemes to verify the convergence. Unfortunately, generation of reasonably regular hexahedral meshes for the problem of interest with our existing software, has turned out to be unrealistic. We had to build a completely new code for tetrahedral meshes from scratch.

A lesson learned from the concentric spheres problem is that we will need higher order elements to cope with the large material contrast.

Experience with the cochlea example indicates the need for a strict monitoring of mesh quality. The scaling analysis indicates that the double precision should be sufficient for solving the problem with a direct multifrontal solver. The encountered numerical singularity occurred in the region of small elements surrounding the cochlea model and indicates a conditioning problem most likely related to a local loss of shape regularity of generated elements.

Appendices

A Formulation of the Coupled Elasticity/Acoustics Problem

In this opening section, we review the derivation of the variational formulations for acoustics, elasticity and then for the ultimate coupled elasticity/acoustics problem.

A.1 Linear Acoustics Equations

The classical linear acoustics equations are obtained by linearizing the isentropic form of the compressible Euler equations expressed in terms of density ρ and velocity vector v_i, around the hydrostatic equilibrium position $\rho = \rho_0, v_i = 0$. Perturbing the solution around the equilibrium position,

$$\rho = \rho_0 + \delta\rho, \quad v_i = 0 + \delta v_i,$$

and linearizing the Euler equations, see e.g. [8], we obtain a system of four first order equations in terms of unknown perturbations of density $\delta\rho$ and velocity δv_i,

$$\begin{cases} (\delta\rho)_{,t} + \rho_0(\delta v_j)_{,j} = 0 \\ \rho_0(\delta v_i)_{,t} + (\delta p)_{,i} = 0\,, \end{cases}$$

with δp denoting the perturbation in pressure. For the isentropic[1] flow, the pressure is simply an algebraic function of density,

$$p = p(\rho)$$

Linearization around the equilibrium position leads to the relation between the perturbation in density and the corresponding perturbation in pressure

$$p = \underbrace{p(\rho_0)}_{p_0} + \frac{dp}{d\rho}(\rho_0)\delta\rho$$

[1] The entropy is assumed to be constant throughout the whole domain

Here p_0 is the hydrostatic pressure, and the derivative $\frac{dp}{d\rho}(\rho_0)$ is interpreted *a posteriori* as the sound speed squared, and denoted by c^2. Consequently, the perturbation in pressure and density are related by the simple linear equation,

$$\delta p = c^2 \delta \rho$$

It is customary to express the equations of linear acoustics in pressure rather than density. Dropping deltas in the notation, we obtain,

$$\begin{cases} c^{-2} p_{,t} & +\rho_0 v_{j,j} & = 0 \\ \rho_0 v_{i,t} & +p_{,i} & = 0 \end{cases}$$

In this report, we shall consider only time-harmonic problems. Assuming ansatz,

$$p(t, \boldsymbol{x}) = e^{i\omega t} p(\boldsymbol{x}), \quad u_i(t, \boldsymbol{x}) = e^{i\omega t} u_i(\boldsymbol{x}) \,,$$

we reduce the acoustics equations to,

$$\begin{cases} c^{-2} i\omega p & +\rho_0 v_{j,j} & = 0 \\ \rho_0 i\omega v_i & +p_{,i} & = 0 \end{cases}$$

or in the operator form,

$$\begin{cases} c^{-2} i\omega p & +\rho_0 \boldsymbol{\nabla} \cdot \boldsymbol{v} & = 0 \\ \rho_0 i\omega v_i & +\boldsymbol{\nabla} p & = 0 \end{cases} \tag{A.1}$$

Eliminating the velocity, we obtain the Helmholtz equation for the pressure,

$$-\Delta p - k^2 p = 0 \,,$$

with the wave number $k = \omega/c$.

Having obtained the second order problem, we can proceed now with the derivation of the weak formulation, as it is usually done in most of text books on the subject. It is a little more iluminating to obtain the same variational formulation starting with the first order system. First of all, we make a clear choice in a way we treat the two equations. The equation of continuity (conservation of mass) is going to be satisfied only in the *weak sense*, i.e. we multiply it with a test function q, integrate over domain Ω and integrate the second term by parts to obtain,

$$\int_\Omega \left(\frac{i\omega}{c^2} pq - \rho_0 \boldsymbol{v} \boldsymbol{\nabla} q \right) d\boldsymbol{x} + \rho_0 \int_\Gamma v_n q \, dS = 0, \quad \forall q \tag{A.2}$$

Here $v_n = v_j n_j$ denotes the normal component of the velocity on the boundary.

The second equation (conservation of momentum) is satisfied in the *strong sense*, i.e. pointwise. Solving for the velocity, we get,

$$\boldsymbol{v} = -\frac{1}{\rho_0 i\omega}\boldsymbol{\nabla} p \tag{A.3}$$

In particular, the normal component of the velocity is related to the normal derivative of the pressure,

$$v_n = -\frac{1}{\rho_0 i\omega}\frac{\partial p}{\partial n}$$

At this point we introduce different boundary conditions:

- a soft boundary Γ_D,
$$p = p_0$$
- a hard boundary Γ_N,
$$v_n = v_0$$
- and an impedance condition with a constant $d > 0$,
$$v_n = dp + v_0$$

Multiplying Equation A.2 with $i\omega$, substituting the boundary data into the boundary term, and eliminating the velocity in the domain integral term, using formula A.3, we get the final variational formulation.

$$\begin{cases} p = p_0 \text{ on } \Gamma_D \\ \displaystyle\int_\Omega \left(\boldsymbol{\nabla} p \boldsymbol{\nabla} q - \left(\frac{\omega}{c}\right)^2 pq \right) d\boldsymbol{x} + i\omega\rho_0 d \int_{\Gamma_C} pq \, dS \;\; = -\int_{\Gamma_N \cup \Gamma_C} v_0 q \, dS \\ \qquad\qquad\qquad\qquad\qquad\qquad\qquad\qquad\qquad\qquad\qquad\qquad \forall q \;:\; q = 0 \text{ on } \Gamma_D \end{cases} \tag{A.4}$$

We have obtained the weak formulation without introducing the second order problem at all! We have a clear understanding which of the starting equations is understood in the weak, and which in a strong sense. The momentum equations, consistently with their pointwise interpretation, have been extended to the boundary to yield the appropriate boundary conditions. We mention only that all these considerations can be made more precise by introducing the language of distributions and Sobolev spaces.

A.2 Linear Elasticity

The time-harmonic linear elasticity equations include:

- balance of momentum,

$$-\rho\omega^2 u_i - \sigma_{ij,j} = f_i$$

- Cauchy displacement-strain relation,

$$\epsilon_{ij} = \tfrac{1}{2}(u_{i,j} + u_{j,i})$$

- consititutive law,

$$\sigma_{ij} = E_{ijkl}\epsilon_{kl}$$

The tensor of elasticities satisfies the usual symmetry assumptions,

$$E_{ijkl} = E_{jikl}, \quad E_{ijkl} = E_{ijlk}, \quad E_{ijkl} = E_{klij}\,.$$

In the case of an isotropic material,

$$E_{ijkl} = \mu(\delta_{ik}\delta_{jl} + \delta_{il}\delta_{jk}) + \lambda\delta_{ij}\delta_{kl}$$

and the constitutive law reduces to the Hooke's law,

$$\sigma_{ij} = 2\mu\epsilon_{ij} + \lambda\epsilon_{kk}\delta_{ij}$$

Utilizing the Cauchy geometric relations, we eliminate the strain tensor and represent the stresses directly in terms of the displacement gradient,

$$\sigma_{ij} = E_{ijkl}u_{k,l} \tag{A.5}$$

or, for the Hooke's law,

$$\sigma_{ij} = \mu u_{i,j} + \lambda u_{k,k}\delta_{ij} \tag{A.6}$$

The momentum equations will be satisfied in the weak sense. We multiply them with a test function v_i, integrate over Ω and integrate by parts to obtain,

$$\int_\Omega \left(\sigma_{ij}v_{i,j} - \rho\omega^2 u_i v_i\right)\, d\boldsymbol{x} - \int_\Gamma \sigma_{ij}n_j v_i\, dS = \int_\Omega f_i v_i\, d\boldsymbol{x}, \quad \forall v_i \tag{A.7}$$

We introduce now the boundary conditions,

- prescribed displacements on Γ_D,

$$u_i = u_{i,D}$$

- prescribed tractions on Γ_N,

$$t_i := \sigma_{ij} n_j = g_i$$

- prescribed impedance on Γ_C,

$$t_i + \beta_{ij} u_j = g_i$$

We restrict ourselves now to $v_i = 0$ on Γ_D, substitute the boundary data into the boundary term in Equation A.7, to obtain,

$$\int_\Omega \left(\sigma_{ij} v_{i,j} - \rho\omega^2 u_i v_i\right)\, d\boldsymbol{x} + \int_{\Gamma_C} \beta_{ij} u_j v_i\, dS = \int_\Omega f_i v_i\, d\boldsymbol{x} + \int_{\Gamma_N \cup \Gamma_C} g_i v_i\, dS \qquad \forall v_i \,:\, v_i = 0 \text{ on } \Gamma_D$$

The final variational formulation is obtained by substituting formula A.5 for stresses,

$$\begin{cases} u_i = u_{i,D} \text{ on } \Gamma_D \\ \displaystyle\int_\Omega \left(E_{ijkl} u_{k,l} v_{i,j} - \rho\omega^2 u_i v_i\right)\, d\boldsymbol{x} + \int_{\Gamma_C} \beta_{ij} u_j v_i\, dS = \int_\Omega f_i v_i\, d\boldsymbol{x} + \int_{\Gamma_N \cup \Gamma_C} g_i v_i\, dS \\ \qquad\qquad \forall v_i \,:\, v_i = 0 \text{ on } \Gamma_D \end{cases} \tag{A.8}$$

We record the final fomulas for the bilinear and linear forms.

$$\begin{aligned} X &= \boldsymbol{H}^1(\Omega) := (H^1(\Omega))^3 \\ b(\boldsymbol{u}, \boldsymbol{v}) &= \int_\Omega \left(E_{ijkl} u_{k,l} v_{i,j} - \rho\omega^2 u_i v_i\right)\, d\boldsymbol{x} + \int_{\Gamma_C} \beta_{ij} u_j v_i\, dS \\ l(\boldsymbol{v}) &= \int_\Omega f_i v_i\, d\boldsymbol{x} + \int_{\Gamma_N \cup \Gamma_C} g_i v_i\, dS \end{aligned} \tag{A.9}$$

A.3 Elasticity Coupled with Acoustics

Let Ω be a domain in $\mathbb{R}^3$. In the following discussion we shall assume that the domain Ω is bounded. We assume that Ω is split into two disjoint parts: a subdomain Ω_e occupied by a linear elastic medium, and a subdomain Ω_a occupied by an acoustical fluid. The two subdomains are separated by an

interface Γ_I. Neither the subdomains nor the interface need to be connected (they may consist of several separate pieces). The external boundary $\partial\Omega$ will be partitioned into Dirichlet, Neumann and Cauchy parts: $\Gamma_D, \Gamma_N, \Gamma_C$, respectively. Each of these boundary parts may consist of a part belonging to the boundary $\partial\Omega_e$ of the elastic subdomain, or the boundary $\partial\Omega_a$ of the acoustical subdomain. Using a more precise mathematical language, Ω_e, Ω_a are assumed to be opened and disjoint and,

$$\overline{\Omega} = \overline{\Omega}_e \cup \overline{\Omega}_a \,.$$

Similarly, elastic and acoustics parts of the Dirichlet boundary: $\Gamma_{De}, \Gamma Da$, of the Neumann boundary: $\Gamma_{Ne}, \Gamma Na$, and the Cauchy boundary: $\Gamma_{Ce}, \Gamma Ca$, are open submanifolds of $\partial\Omega$ and,

$$\partial\Omega = \overline{\Gamma}_{De} \cup \overline{\Gamma}_{Da} \cup \overline{\Gamma}_{Ne} \cup \overline{\Gamma}_{Na} \cup \overline{\Gamma}_{Ce} \cup \overline{\Gamma}_{Ca} \,,$$

as well as,

$$\partial\Omega_e = \overline{\Gamma}_I \cup \overline{\Gamma}_{De} \cup \overline{\Gamma}_{Ne} \cup \overline{\Gamma}_{Ce} \quad \partial\Omega_a = \overline{\Gamma}_I \cup \overline{\Gamma}_{Da} \cup \overline{\Gamma}_{Na} \cup \overline{\Gamma}_{Ca} \,.$$

A two-dimensional illustration of the scenario is shown in Figure 19.

The coupled problem involves solving linear elasticity equations discussed in Section A.2 satisfied in subdomain Ω_e coupled with the equations of linear acoustics discussed in Section A.1 and satisfied in subdomain Ω_a. The unknowns include the components of the displacement vector $u_i(\boldsymbol{x}), \boldsymbol{x} \in \overline{\Omega}_e$ and the acoustical pressure $p(\boldsymbol{x}), \boldsymbol{x} \in \overline{\Omega}_a$. The two sets of equations are accompanied by appropriate boundary conditions and coupled by the following interface conditions:

$$i\omega u_i n_i = v_i n_i = -\frac{1}{\rho_f i\omega}\frac{\partial p}{\partial x_i} n_i, \quad t_i = \sigma_{ij} n_j = -p n_i$$

The first equation above expresses the continuity of normal component of the velocity: the normal elastic velocity has to match the normal component of the acoustical velocity. The second equation expresses the continuity of stresses: the normal elastic stress must be equal to the (negative) pressure, whereas the tangential component of the elastic stress vector is set to zero, since the fluid does not support a shear stress. As usual, ω is the angular frequency, i is the imaginary unit, ρ_f stands for the density of the fluid, and n_i denote components of a unit vector normal to interface Γ_I which we will assume to be directed from the elastic into the acoustical subdomain. Multiplying the first interface condition by $\rho_f i\omega$, we get,

$$\rho_f \omega^2 u_n = \frac{\partial p}{\partial n}, \quad t_i = \sigma_{ij} n_j = -p n_i \tag{A.10}$$

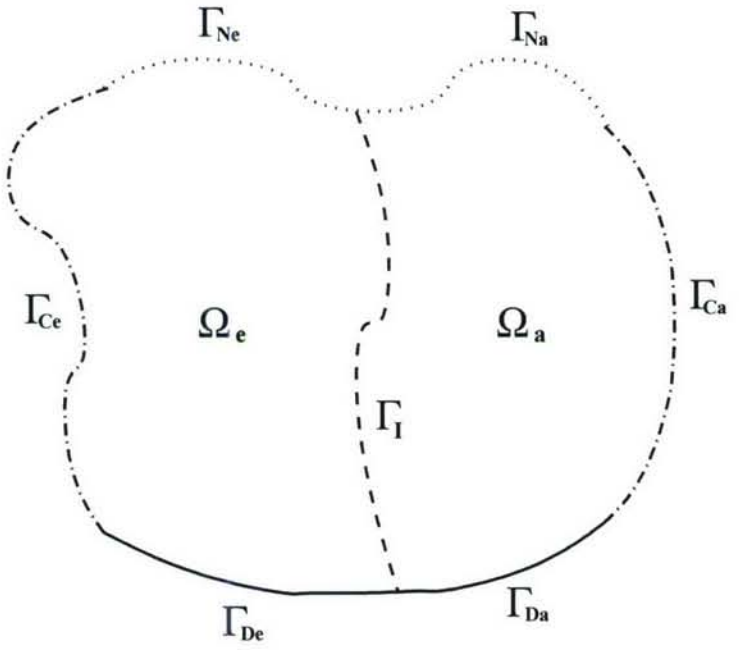

Figure 19: Topology of a coupled problem

where $u_n = u_i n_i$ denotes the normal displacement. From the mathematical point of view, the conditions of this type are classified as *weak coupling conditions*. The word "weak" refers here to the fact that the primary variable for elasticity - the displacement vector, matches the secondary variable (the flux) for the acoustic problem - the normal velocity which is related to the normal derivative of pressure. Conversely, the primary variable for the acoustic problem - the pressure, defines the flux for the elasticity problem. This "cross-coupling" is very essential in proving the well-posedness of the problem, and stability of Galerkin approximations.

On top of the interface conditions we have the usual boundary conditions for acoustics,

- prescribed pressure on Γ_{Da},

$$p = p_D$$

- prescribed normal velocity on Γ_{Na},

$$v_n = v_0$$

- an impedance condition with an impedance constant $d > 0$ on Γ_{Ca},

$$v_n = dp + v_0$$

and for the elasticity,

- prescribed displacements on Γ_{De},

$$u_i = u_{i,D}$$

- prescribed tractions on Γ_{Ne},

$$t_i := \sigma_{ij} n_j = g_i$$

- prescribed impedance on Γ_{Ce},

$$t_i + i\omega\beta_{ij} u_j = g_i$$

We proceed now with the derivation of the variational formulation. We start with the weak form of the continuity equation for acoustics,

$$\int_{\Omega_a} \left(\frac{i\omega}{c^2} pq - \rho_f \boldsymbol{v} \boldsymbol{\nabla} q \right) \, d\boldsymbol{x} + \rho_f \int_{\partial\Omega_a} v_n q \, dS = 0, \quad \forall q$$

and the weak form of the conservation of momentum for elasticity,

$$\int_{\Omega_e} \left(\sigma_{ij} v_{i,j} - \rho_s \omega^2 u_i v_i \right) \, d\boldsymbol{x} - \int_{\partial\Omega_e} \sigma_{ij} n_j v_i \, dS = \int_{\Omega_e} f_i v_i \, d\boldsymbol{x}, \quad \forall v_i$$

with ρ_s and f_i denoting the density of solid and body forces, respectively. Boundary $\partial\Omega_a$ of the acoustic subdomain is now split into the interface Γ_N and parts $\Gamma_{Da}, \Gamma_{Na}, \Gamma_{Ca}$. For the interface Γ_I, we use the first interface condition to replace the flux term $\rho_f v_n$ with $i\omega\rho_f u_n$, and proceed in the standard way with the acoustic boundary conditions, to obtain the variational statement,

$$\begin{cases} p = p_D \text{ on } \Gamma_{Da} \\ \displaystyle\int_{\Omega_a} \left(\frac{i\omega}{c^2} pq + \frac{1}{i\omega} \boldsymbol{\nabla} p \boldsymbol{\nabla} q \right) \, d\boldsymbol{x} + \int_{\Gamma_{Ca}} \rho_f d \, pq \, dS + \int_{\Gamma_I} i\omega\rho_f u_n \, q \, dS = \int_{\Gamma_{Na} \cup \Gamma_{Ca}} \rho_f v_0 q \, dS, \\ \qquad\qquad\qquad\qquad\qquad\qquad\qquad\qquad\qquad\qquad\qquad\qquad \forall q \; : q = 0 \text{ on } \Gamma_{Da} \end{cases}$$

Similarly, boundary $\partial\Omega_e$ of the elastic subdomain is split into the interface Γ_N and parts $\Gamma_{De}, \Gamma_{Ne}, \Gamma_{Ce}$. For the interface Γ_I, we use the second interface condition to replace the flux term $\sigma_{ij}n_j$ with $-pn_i$, and use the boundary conditions to obtain the variational statement,

$$\begin{cases} \boldsymbol{u} = \boldsymbol{u}_D \text{ on } \Gamma_{De} \\ \int_{\Omega_e} \left(E_{ijkl}u_{k,l}v_{i,j} - \rho_s\omega^2 u_i v_i\right)\, d\boldsymbol{x} + i\omega \int_{\Gamma_{Ce}} \beta_{ij}u_j v_i\, dS + \int_{\Gamma_I} pv_n\, dS = \int_{\Omega_e} f_i v_i\, d\boldsymbol{x} + \int_{\Gamma_{Ne}\cup\Gamma_{Ce}} g_i v_i\, dS, \\ \qquad\qquad\qquad\qquad\qquad\qquad\qquad\qquad\qquad\qquad\qquad\qquad \forall \boldsymbol{v} \,:\, \boldsymbol{v} = \boldsymbol{0} \text{ on } \Gamma_{De} \end{cases}$$

Multiplying the variational statement for acoustics by factor $i\omega$, we get the final variational formulation for the coupled problem in the form,

$$\begin{cases} \boldsymbol{u} \in \tilde{\boldsymbol{u}}_D + \boldsymbol{V},\ p \in \tilde{p}_D + V, \\ b_{ee}(\boldsymbol{u}, \boldsymbol{v}) + b_{ae}(p, \boldsymbol{v}) = l_e(\boldsymbol{v}), \quad \forall \boldsymbol{v} \in \boldsymbol{V} \\ b_{ea}(\boldsymbol{u}, q) + b_{aa}(p, q) = l_a(q), \quad \forall q \in V \end{cases} \tag{A.11}$$

where:

- the bilinear and linear forms are given by the formulas:

$$\begin{aligned} b_{ee}(\boldsymbol{u}, \boldsymbol{v}) &= \int_{\Omega_e} \left(E_{ijkl}u_{k,l}v_{i,j} - \rho_s\omega^2 u_i v_i\right)\, d\boldsymbol{x} + i\omega \int_{\Gamma_{Ce}} \beta_{ij}u_j v_i\, dS \\ b_{ae}(p, \boldsymbol{v}) &= \int_{\Gamma_I} pv_n\, dS \\ b_{ea}(\boldsymbol{u}, q) &= -\omega^2\rho_f \int_{\Gamma_I} u_n q\, dS \\ b_{aa}(p, q) &= \int_{\Omega_a} \left(\boldsymbol{\nabla} p \boldsymbol{\nabla} q - k^2 pq\right)\, d\boldsymbol{x} + i\omega \int_{\Gamma_{Ca}} \rho_f d\, pq\, dS \\ l_e(\boldsymbol{v}) &= \int_{\Omega_e} f_i v_i\, d\boldsymbol{x} + \int_{\Gamma_{Ne}\cup\Gamma_{Ce}} g_i v_i\, dS \\ l_a(q) &= i\omega\rho_f \int_{\Gamma_{Na}\cup\Gamma_{Ca}} v_0 q\, dS\,, \end{aligned} \tag{A.12}$$

- $\tilde{\boldsymbol{u}}_D \in \boldsymbol{H}^1(\Omega_e) := (H^1(\Omega_e))^3$ is a finite energy lift of displacements $\boldsymbol{u}_D$ prescribed on Γ_{De}, $\tilde{p_D} \in H^1(\Omega_a)$ is a finite enery lift of pressure p_D prescribed on Γ_{Da},

- $\boldsymbol{V}$ and V are the spaces of the test functions,

$$\begin{aligned} \boldsymbol{V} &= \{\boldsymbol{v} \in \boldsymbol{H}^1(\Omega_e) \,:\, \boldsymbol{v} = \boldsymbol{0} \text{ on } \Gamma_{De}\} \\ V &= \{q \in H^1(\Omega_a) \,:\, q = 0 \text{ on } \Gamma_{Da}\} \end{aligned} \tag{A.13}$$

- $k = \omega/c$ is the acoustic wave number.

Coupled problem A.11 is symmetric if and only if diagonal forms b_{ee} and b_{aa} are symmetric and,

$$b_{ae}(p, \boldsymbol{u}) = b_{ea}(\boldsymbol{u}, p) \, .$$

Thus, in order to enable the symmetry of the formulation[2], we need to rescale problem by, for instance, dividing the second equation by factor $-\omega^2 \rho_f$.

B Finite Element Discretization and Implementation Details

Except for the PML domain, both acoustic and elastic domains are discretized with the simplest linear tetrahedra, i.e. pressure p and elastic displacement components u_i are linear within each element. This implies that all interfaces including the truncating sphere are approximated with plane triangular panels. The triangular mesh on the (approximate) truncating sphere is extended in the radial direction to form two layers of prismatic elements. In order to approximate well the PML induced layer, higher order polynomials in the radial direction are used, $p = 4$ in the first layer, and $p = 2$ in the second layer. This is in accordance with our experience of resolving PML induced boundary layers with *hp*-adaptive elements, see [9] for examples.

B.1 Generation of tetrahedral meshes

We choose an octree-based isocontouring method [16] to extract interior and exterior tetrahedral meshes for the acoustic and elastic domains. First we define the analysis domains and construct a signed distance map. Then a top-down octree subdivision coupled with the dual contouring method is used to rapidly extract adaptive 3D finite element meshes with correct topology from the signed distance map. Finally, the edge contraction and smoothing methods are used to improve the mesh quality. This octree-based technique extends the dual contouring method to crack-free interval volume 3D meshing with feature sensitive adaptation. Compared to other tetrahedral extraction methods from imaging data, this method generates adaptive and quality 3D meshes without introducing any hanging nodes.

At the end, the following files are created:

[2]This is essential, among other reasons, from the point of view of using a direct solver.

- *sphere_file* - contains a list of vertices and triangles on the truncating sphere,
- *tissue_skull_file* - contains a list of vertices and triangles on the tissue/skull interface,
- *air_skull_file* - contains a list of vertices and triangles on the air/skull interface,
- *cochlea_air_file* - contains a list of vertices and triangles on the cochlea/air interface,
- *cochlea_file* - contains a list of vertices and tetrahedra within the cochlea,
- *air_file* - contains a list of vertices and tetrahedra within air,
- *skull_file* - contains a list of vertices and tetrahedra within skull,
- *tissue_file* - contains a list of vertices and tetrahedra within tissue

The meshes are fully compatible, i.e. for instance all vertices for the skull tetrahedra, that are located on the skull/air interface, coicide with vertices listed in *air_skull_file*.

B.2 Data structure and element computations

An existing data structure for higher order hexahedral elements, see [3, 4], has been extended to the case of tetrahedral and prismatic elements. The data structure arrays are initiated with a relevant information on nodal connectivities, and element neighbors necessary for element computations.

Element matrices corresponding to bilinear forms are integrated using standard Gaussian quadrature for tetrahedra (volume integrals) and triangles (interface terms).

B.3 Solvers

Three linear solvers are used in this project. The first one is a serial frontal solver developed at ICES[3], the second one is the European MUMPS, see [10], and the third one is a new, parallel solver enabling solution of large systems of equations with several milions of unknowns, developed especially for this project. Preliminary details on the solver are given in Section C. The

[3]The solver was developed by Dr. Eric Becker, a professor in the ASE/EM Dept. and a long time member of TICOM, next TICAM and now ICES

interfaces with the first two solvers have been implemented for the purpose of verification.

B.4 Graphics

To visualize our models, meshes and solutions, we have implemented a simple interface to the Visualization Toolkit (VTK) [11], a collection of C++ classes that implement a wide range of visualization algorithms. The central data structure for this project is the `vtkUnstructuredGrid`, which represents volumetric data as a collection of points with corresponding scalar values (in this case, the real and imaginary part of the pressure), connected by cells of arbitrary type and dimension (i.e. lines, triangles, quads, tetrahedra, prisms, etc.). This data is then plugged into a variety of filters that allow us to, for example, "slice" through the dataset with a plane to see the pressure in the interior, extract colored isocontours or isosurfaces of the pressure, or generate an animation of the time-dependent pressure $P(x,t) = \mathrm{Re}\,(e^{i\omega t}p(x))$.

C Parallel Linear Solver

The nested-dissections parallel multi-frontal solver is utilized to solve the problem over large meshes. The frontal solver is an extension of the Gaussian elimination, where assembly and elimination are performed together on the so-called frontal sub-matrix of the global matrix [7]. The multi-frontal solver utilizes domain decomposition pattern to work with multiple frontal matrices.

An example of the computational domain related to the head problem, partitioned into 3 sub-domains is presented in Fig. 20. Local orderings of degrees of freedom (d.o.f.) are computed on each sub-domain, where internal d.o.f. are numbered first, and interface d.o.f. are put at the end. Local matrices contain internal d.o.f. interactions part A_i, interface d.o.f. interaction part A_s^i and the interface-internal d.o.f. interaction parts B_i, C_i.

$$\begin{bmatrix} A_i & B_i \\ C_i & A_i^s \end{bmatrix} \begin{bmatrix} x_i \\ x_s^i \end{bmatrix} = \begin{bmatrix} b_i \\ b_s^i \end{bmatrix} \tag{C.1}$$

The global matrix is a sum of local matrices

$$A = \sum_{i=1}^{d} P_i A_i P_i^T. \tag{C.2}$$

Figure 20: Computational mesh partitioned into 3 sub-domains.

The global numbering of d.o.f. is created in the following way:

- All internal d.o.f. from 1-st sub-domain,
- All internal d.o.f. from 2-nd sub-domain,
- ...
- All internal d.o.f. from d-th sub-domain,
- All d.o.f. from the global interface.

The maps P_i are constructed to transfer ordering from local to global. Going into details, let $n =$ denotrs total number of d.o.f.,
$n^{(i)}_{\text{internal}} =$ number of interior d.o.f. of sub-domain i.
$n^{(i)}_{\text{interface}} =$ number of interface d.o.f. of sub-domain i.
$n_{\text{interface}} =$ global number of interface d.o.f..
We define the P_i maps in the following way:

$$P_i : M\left(n^{(i)}_{\text{internal}} + n^{(i)}_{\text{interface}} \times n^{(i)}_{\text{internal}} + n^{(i)}_{\text{interface}}\right) \rightarrow M\left(n \times n\right) \qquad \text{(C.3)}$$

$$P_{bi} : M\left(n^{(i)}_{\text{interface}} \times n^{(i)}_{\text{internal}}\right) \rightarrow M\left(n^{(i)}_{\text{interface}} \times n^{(i)}_{\text{interface}}\right) \qquad \text{(C.4)}$$

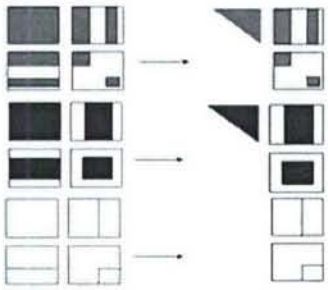

Figure 21: Forward elimination is stopped before processing fake elements. Sub-domain internal nodes are eliminated.

$$P_{ib} : M\left(n^{(i)}_{\text{internal}} \times n^{(i)}_{\text{interface}}\right) \rightarrow M\left(n^{(i)}_{\text{interface}} \times n^{(i)}_{\text{interface}}\right) \tag{C.5}$$

$$P_{bb} : M\left(n^{(i)}_{\text{interface}} \times n^{(i)}_{\text{interface}}\right) \rightarrow M\left(n_{\text{interface}} \times n_{\text{interface}}\right) \tag{C.6}$$

Since

$$P_i A_i P_i^T = \begin{bmatrix} 0 & & & \\ & \cdots & & \\ & & A_i & P_{ib} B_i P_{ib}^T \\ & & \cdots & \\ & & P_{bi} C_i P_{bi}^T & P_{bb} A_s^i P_{bb}^T \end{bmatrix} \begin{bmatrix} x_1 \\ x_2 \\ .. \\ x_d \\ x_s \end{bmatrix} \tag{C.7}$$

the structure of the global stiffness matrix is

$$\begin{bmatrix} A_1 & & .. & & P_{1b} B_1 P_{1b}^T \\ & A_2 & & & P_{1b} B_2 P_{2b}^T \\ & & .. & & .. \\ & & & A_d & P_{db} B_d P_{db}^T \\ P_{b1} C_1 P_{b1}^T & P_{b2} C_2 P_{b2}^T & .. & P_{bd} C_d P_{bd}^T & \sum_{i=1}^{d} P_{bb} A_s^i P_{bb}^T \end{bmatrix} \begin{bmatrix} x_1 \\ x_2 \\ .. \\ x_d \\ x_s \end{bmatrix} = \begin{bmatrix} P_{1b} b_1 P_{1b}^T \\ P_{2b} b_2 P_{2b}^T \\ .. \\ P_{db} b_d P_{db}^T \\ \sum_{i=1}^{d} P_{ib} b_s P_{ib}^T \end{bmatrix}. \tag{C.8}$$

In the 3D code we utilize a serial version of the MUMPS solver [10] over each sub-domain. Single processor versions of MUMPS are executed on each processor for each sub-domain. The MUMPS is executed to provide the Schur complement of the local sub-domain matrix. The internal sub-domain d.o.f. are eliminated with respect to the interface sub-domain d.o.f. The Schur complement of the local system (C.1) for sub-domain i is

$$\hat{A}_i x_s^i = \hat{b}_i \tag{C.9}$$

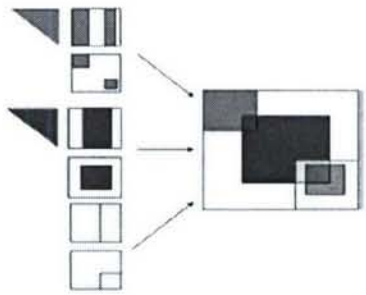

Figure 22: Global interface problem can be aggregated by summing up local Schur complements.

$$\hat{A}_i = A_s^i - C_i A_i^{-1} B_i^T \tag{C.10}$$

$$\hat{b}_i = b_s^i - C_i A_i^{-1} b_i \tag{C.11}$$

A practical way of obtaining the Schur complement is to order d.o.f. in such a way that interface d.o.f. are numbered at the end, and than to execute forward elimination for the internal d.o.f. [13]. The forward elimination is stopped before processing interface d.o.f. After eliminating local internal nodes, the local matrices look like it is presented in Fig. 21 and in (C.12).

$$\begin{bmatrix} U_i & B_i^* \\ 0 & A_i^{s*} \end{bmatrix} \begin{bmatrix} x_i \\ x_s^i \end{bmatrix} = \begin{bmatrix} b_i^* \\ b_s^{i*} \end{bmatrix} \tag{C.12}$$

Once local Schur complements are computed, we can formulate and solve the global interface problem. The Schur complement matrices can be sent to separate process, the global interface problem matrix can be obtained by summing up the local interface matrices, see Fig.22.

$$\hat{A}\hat{x} = \hat{b} \tag{C.13}$$

$$\hat{A} = \sum_{i=1}^{d} P_i A_s^{i*} P_i^T \tag{C.14}$$

$$\hat{b} = \sum_{i=1}^{d} P_i b_s^{i*} P_i^T \tag{C.15}$$

The global interface problem can be solved, by utilizing sequential version of MUMPS, see Fig. 23

$$\hat{A}\hat{x} = \hat{b} \rightarrow \hat{U}\hat{x} = \hat{L}^{-1}\hat{b} \tag{C.16}$$

Figure 23: Global interface problem is solved.

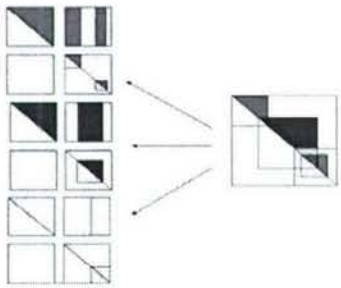

Figure 24: Solution of the global interface problem can be broadcasted into sub-domains.

and the solution can be broadcast into all sub-domains, see Fig. 24. The part of the solution corresponding to local interface node is substituted to the right-hand-side, the identity matrix is put into the right-bottom part of the local matrix

$$\begin{bmatrix} U_i & B_i^* \\ 0 & A_i^{s*} \end{bmatrix} \begin{bmatrix} x_i \\ x_s^i \end{bmatrix} = \begin{bmatrix} b_i^* \\ b_s^{i*} \end{bmatrix} \rightarrow \begin{bmatrix} U_i & B_i^* \\ 0 & 1 \end{bmatrix} \begin{bmatrix} x_i \\ x_s^i \end{bmatrix} = \begin{bmatrix} b_i^* \\ P_{ib}^{T-1} \hat{x} P_{ib}{}^{-1} \end{bmatrix} \tag{C.17}$$

and the backward substitution is executed on sub-domains.

Summing up the presented scheme, to solve the problem distributed into sub-domains, we need to formulate and solve the interface problem first.

For large 3D problems, or for multiple sub-domains, the interface problem is large, its matrix is dense. This motivated us to utilize the idea of nested dissections to reduce computational cost of the interface problem solution. The idea of the nested dissection solver is to utilize the Schur complement pattern recursively. This can be described in the following steps, compare Figure 25.

- In the first step, local internal sub-domain d.o.f. are eliminated with respect to local interface sub-domain d.o.f., in the same way as it is described above.
- Processors are joined into pairs, partial interface matrices are aggre-

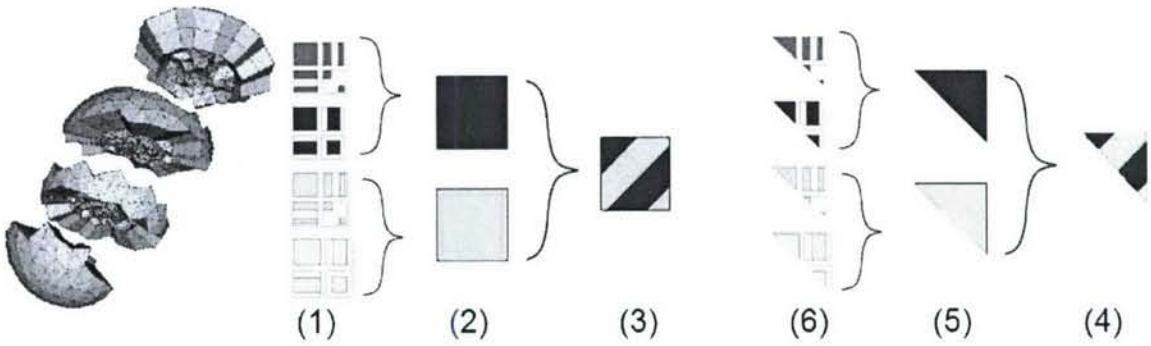

Figure 25: Partial Schur complements (1-2-3) followed by backward substitutions (4-5-6) executed over the nested dissections scheme.

gated for each pair of processors. Common interface d.o.f. are eliminated with respect to external interface d.o.f. within each pair of processors. Notice that this procedure requires to build new interface node numbering within each pair of processors. This is the main technical difficulty in implementing the nested dissection scheme.

- The procedure from the previous step is repeated recursively as long as there are common pieces of interface to be eliminated.
- In the last step of the elimination, there is only one piece of aggregated interface d.o.f. matrix, the common interface part. This interface problem matrix is much smaller, since it corresponds to common part of the interface between two groups of processors. In general, when the domain is not cylindrical, this interface part is associated with the cross-section of the domain. This interface problem can be solved now, since it is much cheaper then the global interface problem in the previous scheme.
- The solution of the common interface part is broadcast back into two group of processors, local solution extracted by using built maps are substituted into Schur complement matrices from current nested dissections step, and the backward substitution is executed to get next contribution to the global interface problem solution.
- The procedure is repeated until we end up with the complete solution of the global interface problem.

Figure 26: Real part of the solution on the simplified model, obtained by parallel execution on 5 processors.

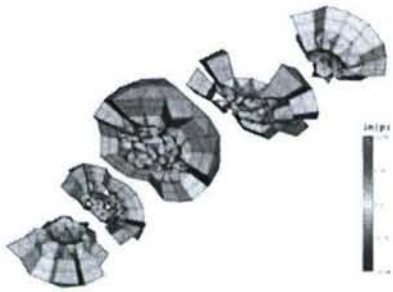

Figure 27: Imaginary part of the solution on the simplified model, obtained by parallel execution on 5 processors.

- In the last step, the backward substitution is executed over sub-domains and the problem is finally solved.

The presented strategy can be easily generalized to the number of processor not equal to the power of 2. The exemplary solution on the simplified model of human head build by concentric spheres is presented in Figures 26 and 27. Because of material data assumed, the maximum solution values are obtained on the skull, compare 28.

The current version of the nested dissection parallel multi-frontal solver attains relative efficiency up to 60 percent.

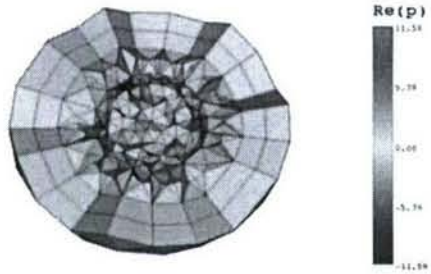

Figure 28: Solution on the central sub-domain, top view.

References

[1] Y.C. Chang and L. Demkowicz. Scattering on a spherical shell problem. Comparison of 3D elasticity and Kirchhoff shell theory results. *Computer Assisted Mechanics and Engineering Science*, 2:207–229, 1995.

[2] Y.C. Chang and L. Demkowicz. A stability analysis for vibrating viscoelastic spherical shells. *Taiwanese Journal of Mathematics*, 2(2):213–242, 1998.

[3] L. Demkowicz. *Computing with hp Finite Elements. I.One- and Two-Dimensional Elliptic and Maxwell Problems.* Chapman & Hall/CRC Press, Taylor and Francis, 2006.

[4] L. Demkowicz, J. Kurtz, D. Pardo, M. Paszyński, W. Rachowicz, and A. Zdunek. *Computing with hp Finite Elements. II. Frontiers: Three-Dimensional Elliptic and Maxwell Problems with Applications.* CRC Press, Taylor and Francis, 2007. in press.

[5] L. Demkowicz and J.T. Oden. Application of hp-adaptive BE/FE methods to elastic scattering. *Comput. Methods Appl. Mech. Engrg.*, 133(3-4):287–318, 1996. a special issue on p and hp methods, edited by I. Babuška and J.T. Oden.

[6] Distmesh - a simple mesh generator in matlab. *http://www-math.mit.edu/ persson/mesh/.*

[7] P. Geng, T. J. Oden, and R. A. Van de Geijn. A parallel multifrontal algorithm and its implementation. *Comput. Methods Appl. Mech. Engrg.*, 149:289–301, 1997.

[8] A. Majda. *Compressible Fluid Flow and Systems of Conservation Laws in Several Space Variables*, volume 53 of *Applied Mathematical Sciences*. Springer-Verlag, New York, 1984.

[9] Ch. Michler, L. Demkowicz, J. Kurtz, and D. Pardo. Improving the performance of perfectly matched layers by means of *hp*-adaptivity. *Numer. Meth. Part. D. E.*, 2007. accepted.

[10] Mumps: a multifrontal massively parallel sparse direct solver. *http://www.enseeiht.fr/lima/apo/MUMPS/*.

[11] W. Schroeder, K. Martin, and B. Lorensen. *The Visualization Toolkit An Object-Oriented Approach To 3D Graphics*. Kitware, Inc. (http://www.kitware.com), 2006.

[12] D. Walsh and L. Demkowicz. *hp* boundary element modeling of the external human auditory system - goal oriented adaptivity with multiple load vectors. *Comput. Methods Appl. Mech. Engrg.*, 192:125–146, 2003.

[13] T. Walsh and L. Demkowicz. A parallel multifrontal solver for *hp*-adaptive finite elements. Technical Report 1, TICAM, The University of Texas at Austin, Austin, TX 78712, 1999.

[14] T. Walsh, L. Demkowicz, and R. Charles. Boundary element modeling of the external human auditory system. *J. Acoust. Soc. Am.*, 115(3), March 2004.

[15] D. Xue, L. Demkowicz, and Ch. Bajaj. Reconstruction of g^1 surfaces with biquartic patches for *hp* FE simulations. In *13th International Meshing Roundtable*, volume 13, pages 323–332, 2004.

[16] Y. Zhang, C. Bajaj, and B-S Sohn. 3D finite element meshing from imaging data. *The special issue of Computer Methods in Applied Mechanics and Engineering (CMAME) on Unstructured Mesh Generation*, 194(48-49):5083–5106, 2005.